Vector optical fields broken in the spatial frequency domain

Xu-Zhen Gao (高旭珍),[1] Yue Pan (潘岳),[1] Si-Min Li,[1] Dan Wang (王丹),[1] Yongnan Li (李勇男),[1] Chenghou Tu (涂成厚),[1,*] and Hui-Tian Wang (王慧田)[1,2,3,†]

[1]*School of Physics and Key Laboratory of Weak-Light Nonlinear Photonics, Nankai University, Tianjin 300071, China*

[2]*National Laboratory of Solid State Microstructures, Nanjing University, Nanjing 210093, China*

[3]*Collaborative Innovation Center of Advanced Microstructures, Nanjing University, Nanjing 210093, China*

(Received 11 January 2016; published 18 March 2016)

We theoretically and experimentally explore the redistribution of polarization states and orbital angular momentum (OAM) in the output plane, induced by the symmetry breaking in the spatial frequency domain. When the vector fields are obstructed by sector-shaped filters in the spatial frequency domain, the local polarization states in the output plane undergo an abrupt transition from linear to circular polarization. The results reveal the polarization-dependent splitting and the appearance of a series of opposite OAMs in the output plane. We also find the self-healing effect of the vector fields broken in the spatial frequency domain and further explore its potential application. If the vector optical fields are used for information transferring or for imaging, even if the optical field carrying the information or image is partially blocked, the complete information or image can still be obtained, implying that which may increase the robustness of the information transferring and the imaging.

DOI: 10.1103/PhysRevA.93.033834

I. INTRODUCTION

As is well known, an optical field can carry spin angular momentum (SAM) and orbital angular momentum (OAM). As an intrinsic nature of light, SAM is associated with polarization and has two possible quantized values of $\pm\hbar$ [1–3], while OAM is associated with the phase front of $\exp(im\varphi)$ where m is called the topological charge [1–7]. Recently, the vector optical fields with the space-variant polarization states, especially cylindrical vector optical fields, have attracted significant interest [8–11] due to their unexpected effects and important applications, such as the far-field focal spot beyond the diffraction limit [8,12–14], the light needle of a longitudinally polarized field [15], the optical cage [16,17], particle acceleration [18], single-molecule imaging [19], near-field optics [20], nonlinear optics [21], optical trapping and manipulation of particles [22,23], and novel angular momentum [22,24].

The symmetry breaking has stimulated substantial research interest due to its decisive role in the origin of substance compared with symmetry [1,24–29]. For example, Davis *et al.* [25] showed the diffraction behavior of a partially blocked scalar vortex field. For the vector optical fields, the symmetry is broken in the original vector optical fields. Wang *et al.* [26] explored the peculiar properties of the local linearly polarized vector optical fields with axial symmetry broken by a sector-shaped filter. Jiao *et al.* [24] reported the redistribution of transverse energy flow and polarization in the vicinity of the focal region, for the azimuthally polarized fields broken by the rotation-symmetric filters in the pupil plane.

In this article, we explore theoretically and experimentally the redistribution of OAM and polarization states in the output plane when the cylindrical vector optical fields are broken by the sector-shaped filters in the spatial frequency plane. We discover some interesting phenomena, such as that the local polarization of the output field undergoes a transition from the linear polarization to the circular one. We also demonstrate that the output fields carry the OAM although the original cylindrical vector optical fields carry no OAM. When studying the propagation properties of the vector fields filtered in the spatial frequency domain, we also find the self-healing effect of the vector fields, which shows the information recovery [30,31] if the partial transverse profile is blocked. Therefore, the property of the information recovery clarifies some potential applications that if the vector optical fields are used for information transferring or for imaging, even if the optical field carrying the information or image is partially blocked, the complete information or image can still be obtained, implying that which may increase the robustness of the information transferring and the imaging.

II. EXPERIMENTAL SETUP

The experimental arrangement for generating, filtering, and reconstructing the vector fields is shown in Fig. 1, which is very similar to those used in Refs. [10,11,32,33]. A 532 nm expanded and collimated laser beam with its linear polarization in the x direction is incident on a spatial light modulator (SLM) placed in the input plane of the first 4f system composed of a pair of identical lenses (L1 and L2) with the same focal length of f. The designed holographic grating (HG) displayed at the SLM diffracts the incoming beam into different diffraction orders. Only $\pm$ first orders are allowed to pass through a spatial filter (with two separate open apertures) placed at the Fourier plane of the first 4f system, and then are converted into two orthogonally polarized beams by a pair of wave plates (WPs) behind the spatial filter, respectively. The $\pm$ first orders are recombined by the Ronchi phase grating (G) placed in the output plane of the first 4f system to generate the demanded vector fields. The output vector optical field illuminates the second 4f system composed of a pair of lenses (L3 and L4) with the different focal lengths. A sector-shaped filter is placed in the spatial frequency plane of the second 4f system to partially hinder the spatial frequency spectra, and a CCD camera is

*tuchenghou@nankai.edu.cn

†htwang@nju.edu.cn/htwang@nankai.edu.cn

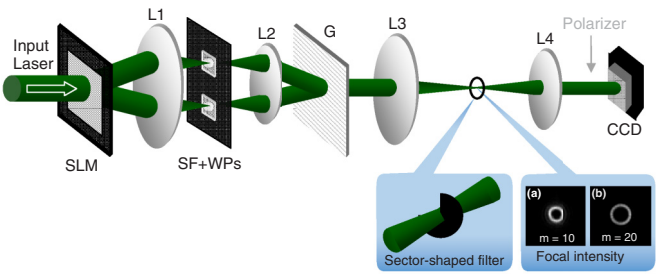

FIG. 1. Schematic of experimental setup. The main configuration is a 4f system composed of a pair of lenses (L1 and L2). A spatial light modulator (SLM) is located in the input plane of the 4f system. Two wave plates (WPs) behind a spatial filter (SF) with two apertures are placed in the spatial frequency plane of the 4f system. A Ronchi phase grating (G) is placed in the output plane of the 4f system. The second 4f system is composed of a pair of lenses (L3 and L4). The left inset is a sector-shaped filter placed in the spatial frequency plane to partially hinder the spatial frequency spectra. The right inset depicts the focal field patterns of the vector fields with (a) $m = 10$ and (b) $m = 20$. The intensity patterns can be recorded by a CCD.

placed in the output plane of the second 4f system to record the output intensity patterns.

III. THEORETICAL DESCRIPTION

The generated cylindrical vector optical fields in the output plane of the first 4f system, with the axial symmetry and with a radius of ρ_0, can be written as [10,11,22]

$$\mathbf{E} = A_0 \mathrm{circ}\left(\frac{\rho}{\rho_0}\right)[\cos(m\varphi - \varphi + \varphi_0)\hat{\mathbf{e}}_\rho + \sin(m\varphi - \varphi + \varphi_0)\hat{\mathbf{e}}_\varphi], \quad (1)$$

where $\hat{\mathbf{e}}_\rho$ and $\hat{\mathbf{e}}_\varphi$ are the unit vectors along the radial and azimuthal directions in the polar system, respectively, and ρ and φ are the polar radius and azimuth angle of the input plane in polar system, respectively. The integer m is the topological charge, φ_0 is the initial phase (within a range of $\varphi_0 \in [-\pi,\pi]$), $\mathrm{circ}(\rho/\rho_0)$ is the circular function, and ρ_0 is the radius of the vector field. A_0 indicates the space-invariant amplitude. With the aid of $\hat{\mathbf{e}}_\rho = (e^{-i\varphi}\sigma^+ + e^{i\varphi}\sigma^-)/\sqrt{2}$ and $\hat{\mathbf{e}}_\varphi = -i(e^{-i\varphi}\sigma^+ - e^{i\varphi}\sigma^-)/\sqrt{2}$, where σ^+ and σ^- stand for the unit vectors of right-handed (RH) and left-handed (LH) circular polarizations, the original vector optical fields can be decomposed, in terms of orthogonal RH and LH circularly polarized components, as

$$\mathbf{E} = \frac{A_0}{\sqrt{2}}\mathrm{circ}\left(\frac{\rho}{\rho_0}\right)[e^{-i(m\varphi+\varphi_0)}\sigma^+ + e^{i(m\varphi+\varphi_0)}\sigma^-]. \quad (2)$$

As φ_0 can change the polarization of the vector field at all points, we can choose $\varphi_0 = 0$ without loss of generality. The focal field of the original vector optical field in the spatial frequency plane can be expressed as

$$\mathbf{E}_f = \frac{A_0}{\sqrt{2}} S_m(r)(-i)^m[e^{-im\theta}\sigma^+ + e^{im\theta}\sigma^-], \quad (3)$$

with

$$S_m(r) = 2\pi \int_0^{\rho_0} \rho J_m\left(\frac{2\pi}{\lambda f} r\rho\right) d\rho,$$

where λ is the wavelength of light in free space and f is the focal length of the lens, r and θ are, respectively, the polar radius and azimuthal angle in the spatial frequency plane (the focal plane is in fact the spatial frequency plane), and $J_m(\cdot)$ is the mth order Bessel function of the first kind.

The amplitude transmission function of the sector-shaped filter in the spatial frequency plane is

$$M(\theta) = \begin{cases} 1 & \theta \in [\theta_0, b+\theta_0) \\ 0 & \text{otherwise} \end{cases}, \quad (4)$$

where θ_0 is the initial position and b is the azimuthal width of the sector-shaped filter, and $M(\theta)$ can be decomposed into a series of Fourier components as follows [26,28,29,34]:

$$M(\theta) = \frac{b}{2\pi}\sum_{n=-\infty}^{+\infty} C_n e^{in\theta} = \frac{b}{2\pi}\sum_{n=-\infty}^{+\infty} \mathrm{sinc}\left(\frac{nb}{2}\right) e^{in(\theta-\frac{b}{2})}. \quad (5)$$

When the spatial frequency spectrum is blocked by a sector-shaped filter, the field in the output plane of the second 4f system can be written as

$$\mathbf{E}_{\mathrm{out}} = \sum_{n=-\infty}^{+\infty} f_n^+(R) e^{-i(m-n)\psi}\sigma^+ + \sum_{n=-\infty}^{+\infty} f_n^-(R) e^{i(m-n)\psi}\sigma^-, \quad (6)$$

where $\exp\{\mp i(m-n)\psi\}$ are the spiral harmonics of the $\pm$ first orders and the coefficient $f_n^\pm(R)$ can be expressed as

$$f_n^+(R) = \frac{A_0}{\sqrt{2}}\frac{b}{2\pi}\mathrm{sinc}\left(\frac{nb}{2}\right) e^{-in(\frac{b}{2}+\frac{\pi}{2})} T_{m-n}(R), \quad (7a)$$

$$f_n^-(R) = \frac{A_0}{\sqrt{2}}\frac{b}{2\pi}\mathrm{sinc}\left(\frac{nb}{2}\right) e^{in(\frac{b}{2}-\frac{\pi}{2})} T_{m-n}(R) \quad (7b)$$

with

$$T_{m-n}(R) = 2\pi \int_0^{r_0} r S_m(r) J_{m-n}\left(\frac{2\pi}{\lambda f} r R\right) dr,$$

where R and ψ are the polar radius and azimuthal angle of the output plane in the polar system, respectively. Clearly, due to the modulation effect of the factor $\mathrm{sinc}(nb/2)$, only $T_m(R)$ (when $n = 0$) is dominant. The output field is consisted of two sectors which rotate in the directions of $\psi = b/2 \pm \pi/2$ due to the existence of $\exp\{\mp in(b/2 \pm \pi/2)\}$ in Eq. (7), implying that the output field is separated into a pair of sectors. Therefore, the filtered focal field with the azimuthal width of b and the bisector in the direction of $\phi = \theta_0 + b/2$ is imaged to form a pair of sector-shaped fields. Such a pair of sector-shaped fields in the output plane of the second 4f system have the same azimuthal width of $\sim b$ and their bisectors are located at the azimuthal directions of $\phi = \theta_0 + b/2 \pm \pi/2$. The two sectors are rotated clockwise and counterclockwise by an angle of $\pi/2$ with respect to the sector-shaped focal field. In particular, such a pair of sector-shaped fields carry not only the opposite SAM (orthogonally RH and LH circular polarizations) but also the opposite OAM of $\pm m\hbar$. Although the output field is composed of a pair of sector-shaped as mentioned above, the

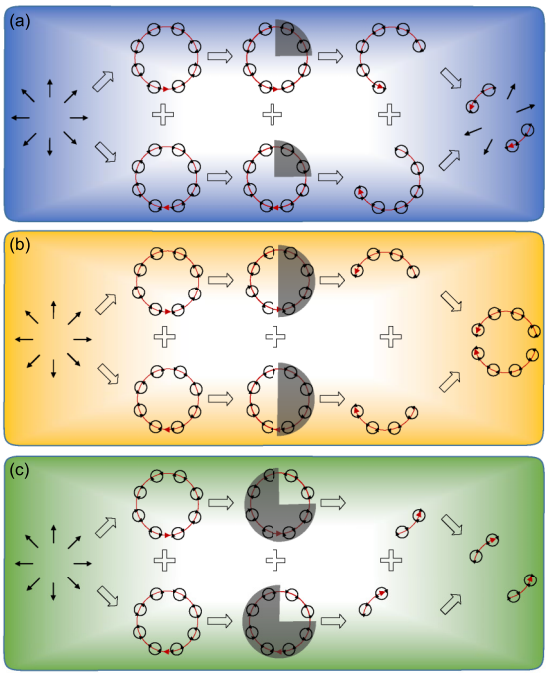

FIG. 2. A diagram for the vector optical fields filtered in the spatial frequency plane. Panels (a), (b), and (c) correspond to the cases of $(b,\theta_0) = (3\pi/2,\pi/2)$, $(\pi,\pi/2)$, and $(\pi/2,0)$, respectively. The first column shows the polarization states of azimuthal-variant local linearly polarized vector fields. The second column shows that the vector fields are a superposition of RH and LH circularly polarized fields (shown by the black circles with arrows) with opposite-sense vortex phases (shown by the red arcs with arrows). The third column shows the spatial frequency plane of $\pm$ first orders blocked by a sector-shaped filter (shown by the gray shadow). The fourthcolumn shows the output $\pm$ first orders. The fifth column shows the output total fields.

sector-shaped fields are in fact not a perfect sector shape due to the diffraction effect of the filter.

To intuitively understand this issue, Fig. 2 as an example shows a diagram for the cylindrical vector optical fields obstructed in the spatial frequency plane by the sector-shaped filters. As is well known, the cylindrical vector fields are composed of RH and LH circularly polarized fields (shown by the black circles with arrows) carrying the opposite-sense vortex phases (shown by the dark red arcs with arrows). The RH and LH circularly polarized fields are rotated by $\pm\pi/2$ with respect to the sector-shaped filter in the spatial frequency plane. The rotation direction depends on the sense of the vortex phase or the OAM. Figure 2(a) shows the case when a quarter occupying the first quadrant in the spatial frequency plane $[(b,\theta_0) = (3\pi/2,\pi/2)]$ is blocked (shown by the gray shadows); the output RH and LH circularly polarized fields occupy the different three quarters. Within the region where two output $\pm$ first orders fields overlap, the field carries no OAM and is local linearly polarized (the SAM is zero) in the output plane. In contrast, within the nonoverlapping region, the two output $\pm$ first orders fields carry still the opposite OAMs and remain the opposite RH and LH circular polarizations. This phenomenon can be understood as follows. In the first and third quadrants, the fields are almost linearly polarized due to the superposition of the RH and LH circularly polarized fields and carry no OAM due to the superposition of the opposite OAMs. In contrast, in the second and fourth quadrants, the fields are RH and LH circularly polarized and carry the opposite OAMs. As in Fig. 2(b), when the spatial frequency plane (the first and fourth quadrants) is blocked by a sector-shaped filter with $(b,\theta_0) = (\pi,\pi/2)$, the fields in the upper-half region (the first and second quadrants) and the lower-half region (the third and fourth quadrants) of the output plane are almost RH and LH circularly polarized and carry the opposite OAMs, respectively. Figure 2(c) shows that when three quarters of the spatial frequency plane is hindered by a sector-shaped filter with $(b,\theta_0) = (\pi/2,0)$, the fields in the first and third quadrants of the output plane are RH and LH circularly polarized and carry the opposite OAMs. Clearly, the symmetry breaking in the spatial frequency plane leads to the redistribution in intensity, polarization state, and OAM in the output plane.

IV. EXPERIMENTS

To verify all the theoretical analysis above, we first explore experimentally the polarization and the intensity distribution of the output fields for the vector optical fields with $m = 10$ and $m = 20$ obstructed by different sector-shaped filters in the spatial frequency plane, with $(b,\theta_0) = (3\pi/2,\pi/2)$, $(\pi,\pi/2)$, and $(\pi/2,0)$. The local polarization states can be obtained by calculating the Stokes parameters (S_0,S_1,S_2,S_3) [35]. In fact, S_0 indicates the total intensity (or normalized total intensity), S_1 or S_2 describes the orientation of polarization (for instance, the direction of linear polarization or the orientation of elliptical polarization), and S_3 stands for the ellipticity and handness of polarization (for $|S_3| = 0$ indicates the linear polarization, $0 < |S_3| < 1$ indicates the elliptical polarization and $|S_3| = 1$ indicates the circular polarization; while the positive and negative S_3 correspond to the RH and LH polarizations, respectively). In Fig. 3, the first, third, and fifth columns show the numerically simulated results for various cases when the vector fields are broken by the different sector-shaped filters in the spatial frequency plane. Here we do not show the Stokes parameter S_2, because it can be derived from the formula of $S_0^2 = S_1^2 + S_2^2 + S_3^2$.

Correspondingly, the experimental results are shown in the second, fourth, and sixth columns of Fig. 3. Clearly, the experimental results are in good agreement with the theoretically expected numerical simulations. For the sake of comparison, the first row of Fig. 3 depicts the Stokes parameters of the locally linearly polarized vector fields in the output plane when the spatial frequency spectra are not broken. The other rows give the Stokes parameters of the output fields for different sector-shaped filters of $(b,\theta_0) = (3\pi/2,\pi/2)$, $(\pi,\pi/2)$ and $(\pi/2,0)$, respectively. As shown in the second row of Fig. 3 $[(b,\theta_0) = (3\pi/2,\pi/2)]$ corresponding to the case of Fig. 2(a), it can be seen that the total intensity of the output field is nonuniform, and the intensity in the first and third quadrants is approximately double of that in the second and fourth quadrants. The measured Stokes parameters, in the fourth and sixth columns of Fig. 3, show that the polarization states in the first and third quadrants are approximately linear polarization, while those in the second and fourth are approximately RH

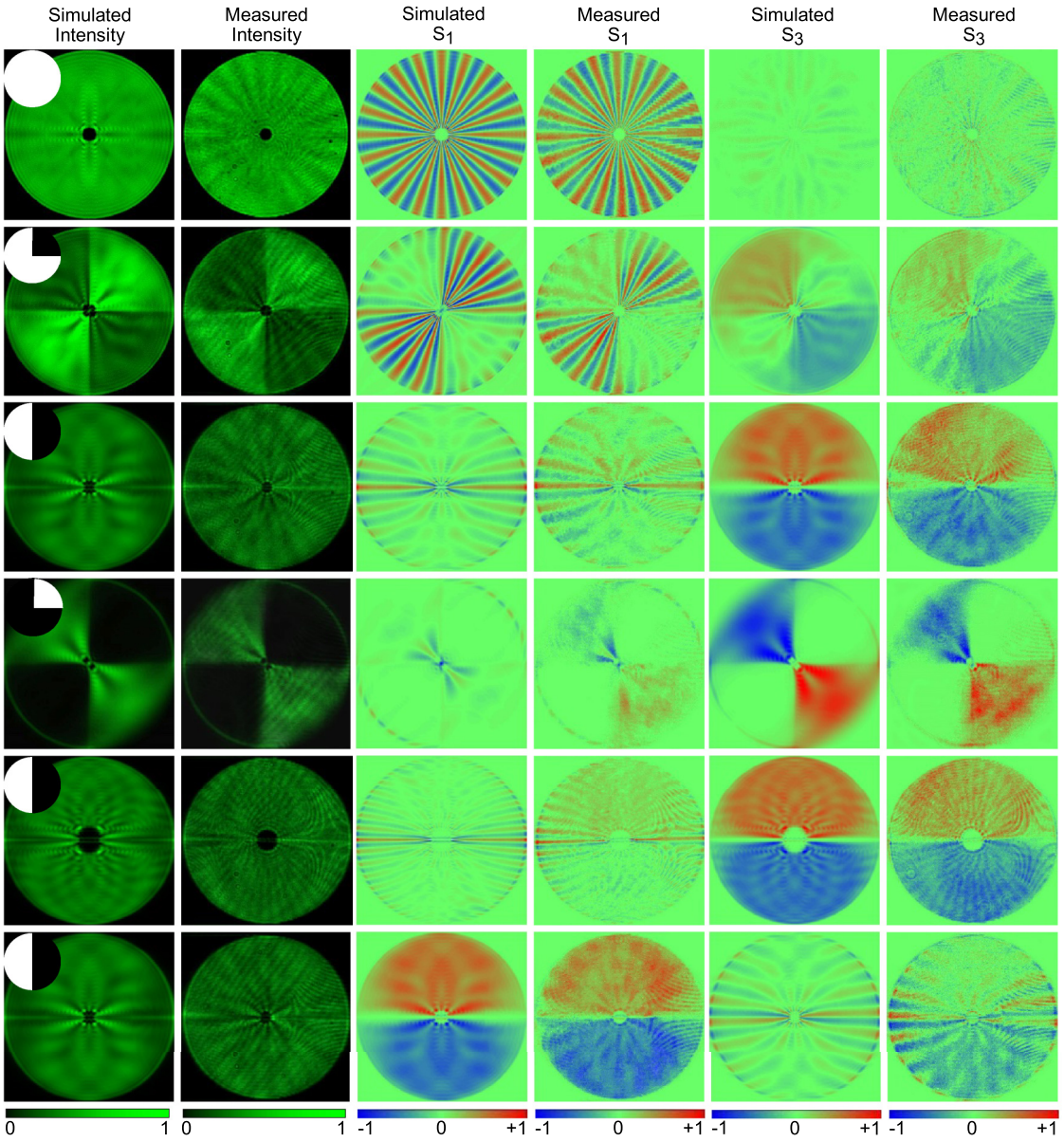

FIG. 3. Intensity patterns of the vector fields with the different sector-shaped filters in the spatial frequency plane and the corresponding Stokes parameters. The first, third, and fifth columns depict the simulated total intensity, Stokes parameters S_1 and S_3 of the output fields, respectively. The second, fourth, and sixth columns give corresponding experimental results. The first, second, third, and fourth rows show the four cases of the original vector fields (generated by a pair of orthogonally circularly polarized bases carrying the opposite OAMs of $m\hbar = \pm 10\hbar$), which are broken by the sector-shaped filters with $(b,\theta_0) = (3\pi/2,\pi/2)$, $(\pi,\pi/2)$, and $(\pi/2,0)$ in the spatial frequency plane, respectively. The fifth row shows the case that the original vector field with $m = 20$ obstructed by a sector-shaped filter with $(b,\theta_0) = (\pi,\pi/2)$ in the spatial frequency plane. The sixth row depicts the case that the original vector field generated by a pair of orthogonally linearly polarized bases carrying the opposite OAMs of $m\hbar = \pm 10\hbar$ is obstructed by the sector-shaped filter with $(b,\theta_0) = (\pi,\pi/2)$ in the spatial frequency plane. The insets in the first column show the corresponding sector-shaped filters used.

and LH circular polarization, respectively. The results in the third and fourth rows correspond to the cases in Figs. 2(b) and 2(c), respectively. The third row shows the case when half of the spatial frequency plane is blocked, the total intensity of the output field is relatively uniform, unlike the second row. The upper and lower half regions of the output fields are nearly RH and LH circularly polarized due to $S_3 \sim 1$ and $S_3 \sim -1$, respectively. The fourth row shows the case when only the first quarter in the spatial frequency plane is allowed to pass, and the intensity pattern of the output field is nonuniform, where the intensity almost vanishes in the first and third quadrants. The output field in the second and fourth quadrants are LH and RH circularly polarized with $S_3 \sim -1$ and $S_3 \sim 1$, respectively. The fifth row shows the case when a vector field with $m = 20$ is obstructed by a sector-shaped filter with $(b,\theta_0) = (\pi,\pi/2)$ in the spatial frequency plane. Except that the polarization singularity in the center becomes larger than the above vector fields with $m = 10$, the distributions of intensity and polarization states have no essential difference from the case shown in the third row.

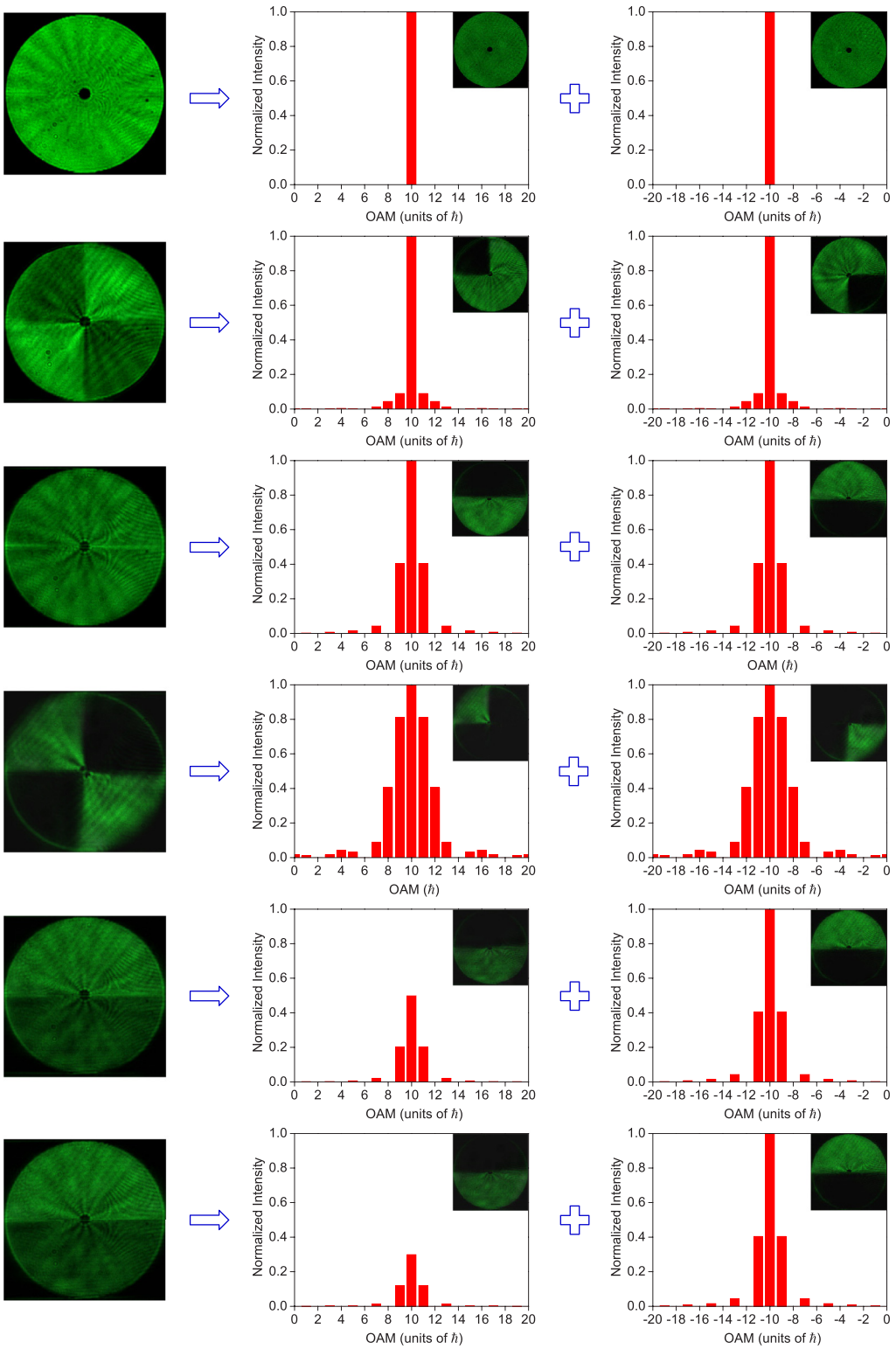

FIG. 4. The total intensity and the numerically simulated OAM spectra of the output fields, when the original vector optical fields generated by a pair of orthogonal circularly polarized base vectors carrying the opposite OAMs of $m\hbar = \pm 10\hbar$ are broken by different sector-shaped filters in the spatial frequency plane. The first column depicts the intensity patterns of the output fields, while the second and third columns show the OAM spectra of $\pm$ first orders, respectively. The first, second, third, and fourth rows show the cases, where the same original vector fields are generated by a pair of equal-intensity orthogonally circularly polarized base vectors carrying the opposite OAMs of $m\hbar = \pm 10\hbar$, while they are obstructed by the different sector-shaped filters with $(b,\theta_0) = (2\pi,0)$, $(3\pi/2,\pi/2)$, $(\pi,\pi/2)$, and $(\pi/2,0)$ in the spatial frequency plane, respectively. The fifth and sixth rows depict the cases where original vector fields are generated by a pair of unequal-intensity orthogonally circularly polarized base vectors carrying the opposite OAMs of $m\hbar = \pm 10\hbar$, with $T = 0.5$ and 0.3, respectively, while the same sector-shaped filter with $(b,\theta_0) = (\pi,\pi/2)$ is used. Insets: the measured output intensity patterns of $\pm$ first orders.

Differently from the above five rows, in which their original vector fields are generated by a pair of orthogonally RH and LH circularly polarized bases carrying the opposite OAMs, the sixth row depicts a case that the original vector field is generated by a pair of orthogonally linearly polarized bases carrying the opposite OAMs with $m = \pm 10$. In the sixth row, the field in the spatial frequency plane is filtered by the sector-shaped filter with $(b,\theta_0) = (\pi,\pi/2)$. The polarization states of the output field in the first and second (third and fourth) quadrants are almost $+45^\circ$ (-45°) linear polarization located at the point $(S_1,S_2,S_3) = (1,0,0)$ [$(S_1,S_2,S_3) = (-1,0,0)$] in the equator on the Poincaré sphere. This is similar to the above phenomena. We can see from the results above that the $\pm$ first orders will experience the spin-dependent splitting in the redistribution process, undergoing anticlockwise and clockwise rotation at $\pi/2$, respectively. In particular, there is no significant difference in the splitting behavior of spin components for the vector fields with higher order modes and different orthogonally polarized bases.

We have analyzed the polarization redistribution of the output fields by showing the Stokes parameters in the above. In order to further explore the field structure in the output plane, we now will discuss the OAM intensity spectrum of the $\pm$ first orders, which means the distribution of the helical-harmonic magnitudes over the summation index n. From Eqs. (6) and (7), we can find that the central OAMs of $\pm$ first orders are $\pm m\hbar$, and the OAM of the incident light acquires OAM spectrum shifted by n, generating new OAM sidebands. The OAM intensity spectra of the $\pm$1st orders are described by $|f_n^+(R)|^2$ and $|f_n^-(R)|^2$, respectively. It should be pointed out that the OAM spectra of the incident light transmitted through a sector-shaped filter have a sinc^2-form envelope, and the OAM spectra are discrete owing to the periodic boundary condition in the azimuthal dimension. Then we perform with Eqs. (6) and (7) the numerical simulations for the normalized OAM spectra, as shown in Fig. 4, which are in good agreement with those predicted. For the case of no filter, there has no change in OAMs of the $\pm$ first orders which are completely opposite ($\pm 10\hbar$) and not separated in space, as shown in the 1st row of Fig. 4. The second, third, and fourth rows show the OAM spectra when the fields are blocked by the sector-shaped filters with $(b,\theta_0) = (3\pi/2,\pi/2)$, $(\pi,\pi/2)$, and $(\pi/2,0)$ in the spatial frequency plane, respectively. It can been found that the OAM will be spread (i.e., the OAM spectra become more rich) as the size b of the filter decreases. This phenomenon is easily explained based on Heisenberg's uncertainty principle for the angular position and the OAM. The OAM intensity spectra are determined by the Fourier transform of the angular distribution [28,29,34]. The total intensity patterns in the first column of Fig. 4 is the same as Fig. 3, while the measured intensity patterns of $\pm$ first orders of the output fields corresponding to the OAM spectra are shown in the insets in Fig. 4.

We also explore the cases when the original vector fields are generated by a pair of orthogonally polarized components, which carry the opposite OAMs of $m = \pm 10$ but have the different intensity (T defines the relative intensity fraction) [36]. The fifth and sixth rows of Fig. 4 show two cases of $T = 0.5$ and 0.3, in which both are broken by the same sector-shaped filter with $(b,\theta_0) = (\pi,\pi/2)$ in the spatial frequency plane, respectively. The OAM spectrum of the $+$ first order remains almost to be unchanged, while the weight of the OAM spectrum of the $-$ first order is only 50% and 30% (which equals to T) of that of the $+$ first order. In addition, as shown by the insets in the fifth and sixth rows, the intensity of the output fields in the upper and lower half regions are also different, with the intensity ratio being equal to the corresponding values of T.

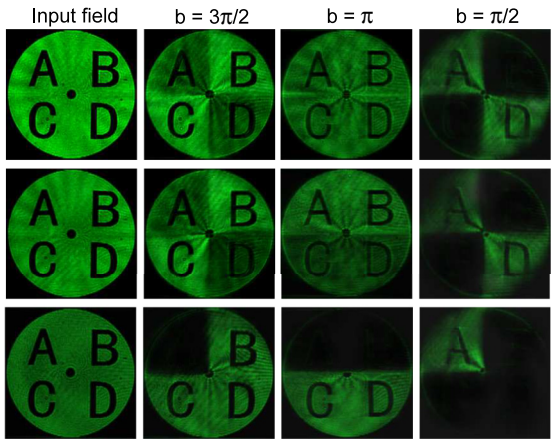

FIG. 5. The intensity patterns of the output fields for the original vector optical fields with "A, B, C, D" alphabets obstructed by the sector-shaped filter in the spatial frequency plane. The first and second rows depict the cases of original vector fields composed of orthogonally circularly polarized base vectors with the opposite OAMs of $m\hbar = \pm 10\hbar$ when with $T = 1$ and $T = 0.5$, respectively. As a comparison, the 3rd row depicts the case of scalar optical field with the OAM of $m\hbar = 10\hbar$. The second, third, and fourth columns show the three cases of the sector-shaped filters with $(b,\theta_0) = (3\pi/2,\pi/2)$, $(\pi,\pi/2)$, and $(\pi/2,0)$ in the spatial frequency plane, respectively.

In the above, we focus only on the spatial structures of the polarization states and OAM of the output fields. However, it is also of great importance to explore some potential applications. As shown in Fig. 2, when the vector fields are broken in the spatial frequency plane, the fields in the output plane can be strangely recovered under some special conditions. We explore now the ability of information recovering when the information we want to transfer is disturbed or distorted. We store the information in amplitude of the vector fields. As an example, four letters "A, B, C, D" are loaded in the amplitude of the original vector fields as the information. The first (second) row in Fig. 5 corresponds to the case that the information is loaded on the original vector field generated by a pair of equal-intensity (unequal-intensity, $T = 0.5$) orthogonally polarized bases with the opposite OAMs of $\pm 10\hbar$. As shown in the second and third columns, in which the fields in the spatial frequency plane are obstructed by 1/4 ($b = 3\pi/2$) and 1/2 ($b = \pi$), respectively, all the four letters "A, B, C, D" can be still recovered in the output plane despite the intensity exhibiting some nonuniformity. As shown in the fourth column, however, when the fields are filtered by a sector-shaped filter with $b = \pi/2$ in the spatial frequency plane, the output fields include only "A" and "D." As a comparison, we also explore the case of the scalar optical

FIG. 6. The intensity patterns for three kinds of vector optical fields with the Nankai university logo obstructed by a sector-shaped filter with $(b,\theta_0) = (\pi,\pi/2)$ in the spatial frequency plane. The first row shows three kinds of original vector fields, while the second row depicts the corresponding output fields. The first, second, and third columns correspond to the original vector fields with $(m,T) = (10,1)$, $(20,1)$, and $(10,0.3)$, respectively.

field carrying the same information of "A, B, C, D," as shown in the third row. This scalar optical field is the − first order of the vector field used in the first row, which is in fact a circularly polarized vortex optical field with the OAM of $10\hbar$. We can find from the third row in Fig. 5 that the information of the scalar field cannot be recovered clearly, though there may occur fuzzy dark information if you look carefully. These results show the ability of information recovery in the output plane even if the part of the vector field in the spatial frequency plane is blocked.

We also attempt the recovery of more complicated information. Here we choose the logo of our university as the transferred information, which is carried by three vector fields, respectively. The three original vector fields carrying the information are shown by three images in the first row of Fig. 6, respectively. We explore the influence of different original vector fields on the quality of the recovered information. It should be pointed out that all the three fields are filtered by a sector-shaped filter with $(b,\theta_0) = (\pi,\pi/2)$ in the spatial frequency plane. In the second row, the corresponding output fields are shown. The first, second, and third columns correspond to the three vector fields: (1) the first one is generated by a pair of equal-intensity orthogonally polarized bases carrying the opposite OAMs of $\pm 10\hbar$, (2) the second one has only a difference from the 1st one that the opposite OAMs are changed into $\pm 20\hbar$, and (3) the third one has only a difference from the first one in that the intensity ratio is changed from $T = 1$ into $T = 0.5$, respectively. From these experimental results, we can find that more complicated information can also be recovered if only the obstructed field in the spatial frequency plane is not beyond a half, no matter what parameters of the vector fields we chose. This result extends our understanding of the vector fields in information communications and may increase robustness of information transmission. We should point out that if the noise is the phase-only form, under the situation of strong phase-only noise, it should be very difficult to well recover the information; while under the situation of weak phase-only noise, it is possible to better recover the information. In contrast, if the noise is the amplitude-only form, as long as the obstructed area is not beyond a half, it is able to completely recover the information.

V. CONCLUSION

In summary, we have investigated theoretically and experimentally the redistribution of OAM and polarization states of the output fields for the vector optical fields broken in the spatial frequency plane by the sector-shaped filters. When the spatial frequency spectrum of the cylindrical vector optical fields is blocked, there occur spin-dependent splitting and a series of opposite OAMs in the output field. Besides the propagation behaviors of the vector fields broken in the spatial frequency domain, we also find the self-healing effect of the vector fields broken in the spatial frequency domain. We also further explore its potential application. As long as the obstructed vector field in the spatial frequency domain is not beyond a half, even more complicated information carried in the amplitude of the original vector field can be recovered. This means the vector optical fields can be used for information transferring or for imaging, even if the optical field carrying the information or image is partially blocked, the complete information or image can still be obtained, implying that which may increase the robustness of the information transferring and the imaging.

ACKNOWLEDGMENTS

This work is supported by the 973 Program of China under Grant No. 2012CB921900, the National Natural Science Foundation of China under Grants Nos. 11534006, 11274183, and 11374166, and the National Scientific Instrument and Equipment Development project 2012YQ17004.

[1] M. Padgett, J. Courtial, and L. Allen, Phys. Today **57**(5), 35 (2004).
[2] L. Allen, M. J. Padgett, and M. Babiker, Prog. Opt. **39**, 291 (1999).
[3] Y. Q. Zhao, J. S. Edgar, G. D. M. Jeffries, D. McGloin, and D. T. Chiu, Phys. Rev. Lett. **99**, 073901 (2007).
[4] L. Allen, M. W. Beijersbergen, R. J. C. Spreeuw, and J. P. Woerdman, Phys. Rev. A **45**, 8185 (1992).
[5] G. Molina-Terriza, J. P. Torres, and L. Torner, Nat. Phys. **3**, 305 (2007).
[6] A. T. O'Neil, I. MacVicar, L. Allen, and M. J. Padgett, Phys. Rev. Lett. **88**, 053601 (2002).
[7] J. E. Curtis and D. G. Grier, Phys. Rev. Lett. **90**, 133901 (2003).
[8] Q. W. Zhan, Adv. Opt. Photon. **1**, 1 (2009).
[9] C. Maurer, A. Jesacher, S. Fürhapter, S. Bernet, and M. Ritsch-Marte, New J. Phys. **9**, 78 (2007).

[10] X. L. Wang, J. P. Ding, W. J. Ni, C. S. Guo, and H. T. Wang, Opt. Lett. **32**, 3549 (2007).
[11] X. L. Wang, Y. N. Li, J. Chen, C. S. Guo, J. P. Ding, and H. T. Wang, Opt. Express **18**, 10786 (2010).
[12] R. Dorn, S. Quabis, and G. Leuchs, Phys. Rev. Lett. **91**, 233901 (2003).
[13] K. S. Youngworth and T. G. Brown, Opt. Express **7**, 77 (2000).
[14] X. Hao, C. F. Kuang, T. T. Wang, and X. Liu, Opt. Lett. **35**, 3928 (2010).
[15] H. F. Wang, L. P. Shi, B. Lukyanchuk, C. Sheppard, and C. T. Chong, Nat. Photon. **2**, 501 (2008).
[16] Y. Kozawa and S. Sato, Opt. Lett. **31**, 820 (2006).
[17] X. L. Wang, J. Ding, J. Q. Qin, J. Chen, Y. X. Fan, and H. T. Wang, Opt. Commun. **282**, 3421 (2009).
[18] C. Varin and M. Piche, Appl. Phys. B **74**, 83 (2002).
[19] L. Novotny, M. R. Beversluis, K. S. Youngworth, and T. G. Brown, Phys. Rev. Lett. **86**, 5251 (2001).
[20] A. Ciattoni, B. Crosignani, P. Di Porto, and A. Yariv, Phys. Rev. Lett. **94**, 073902 (2005).
[21] A. Bouhelier, M. Beversluis, A. Hartschuh, and L. Novotny, Phys. Rev. Lett. **90**, 013903 (2003).
[22] X. L. Wang, J. Chen, Y. N. Li, J. P. Ding, C. S. Guo, and H. T. Wang, Phys. Rev. Lett. **105**, 253602 (2010).
[23] Q. W. Zhan, Opt. Express **12**, 3377 (2004).
[24] X. Y. Jiao, S. Liu, Q. Wang, X. T. Gan, P. Li, and J. L. Zhao, Opt. Lett. **37**, 1041 (2012).
[25] J. A. Davis and J. B. Bentley, Opt. Lett. **30**, 3204 (2005).
[26] X. L. Wang, K. Lou, J. Chen, B. Gu, Y. N. Li, and H. T. Wang, Phys. Rev. A **83**, 063813 (2011).
[27] S. Vyas, M. Niwa, Y. Kozawa, and S. Sato, J. Opt. Soc. Am. A **28**, 1387 (2011).
[28] S. Franke-Arnold, S. M. Barnett, E. Yao, J. Leach, J. Courtial, and M. Padgett, New J. Phys. **6**, 103 (2004).
[29] B. Jack, M. J. Padgett, and S. Franke-Arnold, New J. Phys. **10**, 103013 (2008).
[30] T. Bauer, S. Orlov, U. Peschel, P. Banzer, and G. Leuchs, Nat. Photon. **8**, 23 (2014).
[31] A. Lubk, G. Guzzinati, F. Börrnert, and J. Verbeeck, Phys. Rev. Lett. **111**, 173902 (2013).
[32] Y. Pan, S. M. Li, L. Mao, L. J. Kong, Y. N. Li, C. H. Tu, P. Wang, and H. T. Wang, Opt. Express **21**, 16200 (2013).
[33] Y. Pan, Y. N. Li, S. M. Li, Z. C. Ren, Y. Si, C. H. Tu, and H. T. Wang, Opt. Lett. **38**, 3700 (2013).
[34] E. Yao, S. Franke-Arnold, J. Courtial, S. Barnett, and M. Padgett, Opt. Express **14**, 9071 (2006).
[35] Z. Bomzon, M. Gu, and J. Shamir, Appl. Phys. Lett. **89**, 241104 (2006).
[36] Y. Pan, Y. N. Li, Z. C. Ren, Y. Si, C. H. Tu, and H. T. Wang, Phys. Rev. A **89**, 035801 (2014).